

Dual-Scale Stick-Slip Friction on Graphene/*h*-BN Moiré Superlattice Structure

Shuai Zhang^{1,2}, Quanzhou Yao^{1,2}, Lingxiu Chen³, Chengxin Jiang^{4,5}, Tianbao Ma², Haomin Wang^{4,*},
Xi-Qiao Feng^{1,2} and Qunyang Li^{1,2,†}

¹Applied Mechanics Laboratory, Department of Engineering Mechanics, Tsinghua University, Beijing 100084, China

²State Key Laboratory of Tribology, Tsinghua University, Beijing 100084, China

³School of Materials Science and Physics, China University of Mining and Technology, Xuzhou 221116, China

⁴State Key Laboratory of Functional Materials for Informatics, Shanghai Institute of Microsystem and Information Technology, Chinese Academy of Sciences, Shanghai 200050, China

⁵School of Physical Science and Technology, ShanghaiTech University, Shanghai 201210, China

 (Received 27 October 2021; revised 22 January 2022; accepted 6 May 2022; published 2 June 2022)

Using atomic force microscopy, we have shown that friction on graphene/*h*-BN superlattice structures may exhibit unusual moiré-scale stick slip in addition to the regular ones observed at the atomic scale. Such dual-scale slip instability will lead to unique length-scale dependent energy dissipation when the different slip mechanisms are sequentially activated. Assisted by an improved theoretical model and comparative experiments, we find that accumulation and unstable release of the in-plane strain of the graphene layer is the key mechanism underlying the moiré-scale behavior. This work highlights the distinct role of the internal state of the van der Waals interfaces in determining the rich dynamics and energy dissipation of layer-structured materials.

DOI: [10.1103/PhysRevLett.128.226101](https://doi.org/10.1103/PhysRevLett.128.226101)

Stick slip is an interesting yet intricate friction phenomenon widely observed for sliding interfaces ranging from atomic to geological scale [1–7]. Among the stick-slip behaviors, atomic-scale stick slip, commonly examined with atomic force microscopy (AFM), has attracted much attention due to its close relation with the origins of friction and the fundamental mechanisms of energy dissipation [8–18]. Historically, atomic stick-slip friction has been interpreted by the Prandtl-Tomlinson (*P-T*) model [19,20], where a particle is driven by a linear spring to slide on a periodic energy landscape. In atomic stick-slip friction experiments, the energy landscapes are typically constant with steady-state slip forces [2,8,11,15]; however, there do exist a few exceptions where the energy landscape appears to vary with multiple periodicity. For example, when an AFM tip sliding on surfaces with atomic reconstructions [21] or surfaces of heterostructures [22–26], a long-period modulation on the lateral energy landscape can be found. In this Letter, we demonstrated that, when sliding a nanoscale tip on graphene/*h*-BN heterostructure with a moiré pattern, stick slip could occur both at the atomic scale and at the moiré scale. Because of this unique dual-scale stick-slip behavior, different energy dissipation channels with distinct dissipation rates could be sequentially activated by changing the scan size. More surprisingly, we found that the magnitude of the moiré-scale stick slip was smaller than that of the atomic stick slip, which directly contradicted the predictions from the classic models with a fixed energy landscape [10,27]. To resolve this, we proposed an improved *P-T* model by incorporating the elastic strain energy of graphene layer

and the graphene/*h*-BN interfacial interaction energy induced by the tip pressure, both of which were coupled with the tip position. The improved *P-T* model shows that the unusual moiré-scale stick slip originates from local unstable slip of graphene rather than the tip in contrast to the classic *P-T* models.

Figure 1(a) schematically shows the experimental setup, where an AFM was used to measure friction on surfaces of graphene/*h*-BN heterostructures. In our experiments, the single-crystal monolayer graphene islands with typical diameters around 10 μm were grown on bulk *h*-BN substrate (more details of the sample are shown in Supplemental Material, Fig. S1 [28]). According to the period of the moiré structure obtained from scanning tunneling microscopy (STM) and lattice-resolved AFM images (see Supplemental Material, Fig. S2 [28]), the crystalline orientation of the graphene layer is aligned with the *h*-BN substrate. As shown in the upper panel of Fig. 1(b), the lateral force image of this sample exhibits a clear hexagonal pattern with a period of ~ 15 nm, consistent with the period of the moiré structure. From the lateral force traces [lower panel of Fig. 1(b)], we can see that this hexagonal pattern originates from a series of moiré-scale stick-slip events, which are found to be insensitive to the sliding velocity (Supplemental Material, Fig. S3 [28]). When the lateral force image is further enlarged, as shown in Figs. 1(c) and 1(d), atomic-scale stick slip with a period corresponding to the graphene lattice can also be well recognized. As energy dissipation is often closely associated with stick-slip motion, the dual-scale stick-slip behavior might lead to

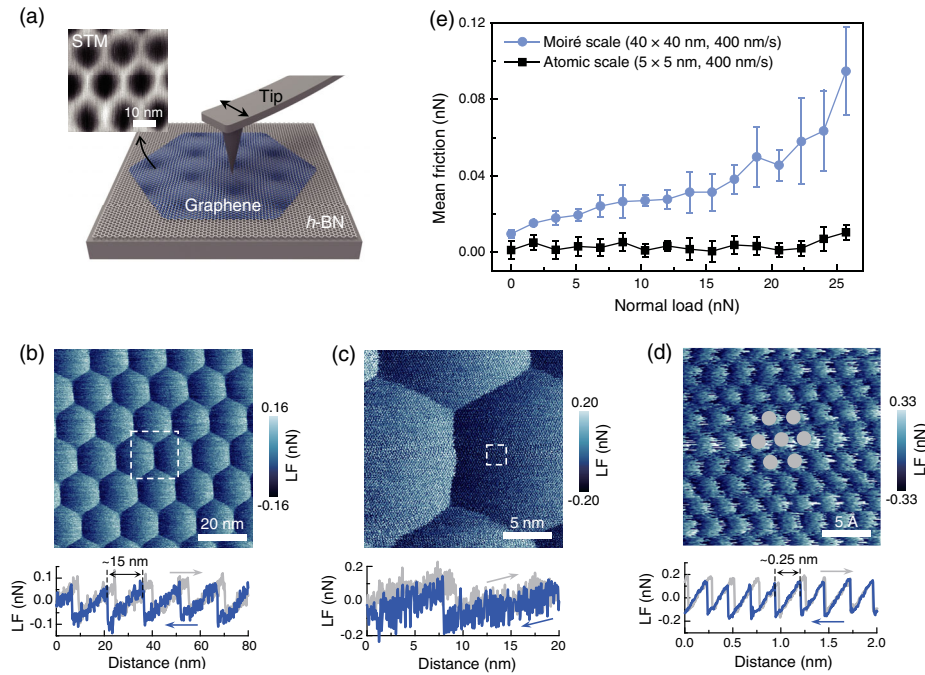


FIG. 1. (a) A schematic of the friction measurement. The inset shows the moiré pattern with a period of ~ 15 nm obtained from STM. (b) Lateral force image (upper panel) and the corresponding line traces (lower panel) show a hexagonal pattern originating from moiré-scale stick slip. Scale bar, 20 nm. (c) Close-up lateral force image (upper panel) and the corresponding line traces (lower panel) acquired from the dashed rectangle region of panel (b). Scale bar, 5 nm. (d) Close-up lateral force image (upper panel) and the corresponding line traces (lower panel) acquired from the dashed rectangle region of panel (c). Scale bar, 5 Å. (e) Friction versus normal load data acquired from areas with 5 nm \times 5 nm (atomic-scale) and 40 nm \times 40 nm (moiré-scale) sizes. Error bars represent the standard deviation at each load. As the typical size of the graphene islands was much larger than the tip contact size (\sim a couple of nm), we did not expect them to move or rotate globally with respect to the *h*-BN substrate.

length-scale dependent energy dissipation rates. To test this idea, we conducted friction tests under two different scan sizes. As shown in Fig. 1(e), when the scan size is relatively small and only atomic-scale stick slip is activated, the mean friction remains at a low level around 0.005 nN (see more details in Supplemental Material, Fig. S4 [28]). However, when the scan size is large enough to accommodate the moiré-scale stick slip, mean friction increases significantly (nearly 10 times).

Previously, a long-range modulation effect on the atomic stick-slip friction has been reported for reconstructed Au(111) surface [21] and graphene/Ru or graphene/Pt heterostructures [22,24]. Such modulation effect was believed to be caused by local topographical undulations due to out-of-plane buckling of the top atomic layer [22,29], or in-plane straining of graphene due to strong pinning between graphene layer and the substrate [24]. However, because the interlayer interaction is relatively weak for graphene/*h*-BN sample [30,31], its height fluctuation is only ~ 1 Å (see Supplemental Material, Fig. S2 [28]), which is unlikely to cause the significant moiré-scale stick slip. To capture the long-range modulation effect, the classic *P-T* model was often adopted by considering a dual-scale energy potential including both atomic-scale corrugation and long-range modulations

[21,22,24,25]. Based on the model predictions [10,27], stick-slip behavior only occurs when the normalized energy corrugation is large enough, i.e., $2E_0\pi^2/ka^2 > 1$, where E_0 and a are the amplitude and the period of the energy corrugation, k is the stiffness of the spring. Since the period of the moiré pattern (~ 15 nm) is much larger than that of the graphene lattice (~ 0.25 nm), to have atomic and moiré scale stick slip simultaneously, the amplitude of the moiré-scale energy corrugation should be ~ 3600 times larger than that of the atomic-scale energy corrugation. Consequently, the fluctuation of the lateral force at the moiré scale would also be ~ 3600 larger, which directly contradicts the experimental observations [see Figs. 1(b) and 1(d)].

As the moiré-scale friction exhibits unusually strong dependence in load [Fig. 1(e)], we further examined the variation trend of the moiré-scale friction while systematically changing the load. As shown by the representative friction loops in Fig. 2(a), when normal load increases, the moiré-scale stick slip becomes more pronounced with higher peak slip forces, indicating more energy dissipation. In addition, we found that the shape of the moiré patterns also changes noticeably with normal load as indicated in Fig. 2(b). For example, a regular hexagonal moiré pattern can be observed at relatively small loads (e.g., at 1.4 or 5.7 nN). However, as the load increases to 25.7 nN, the unit

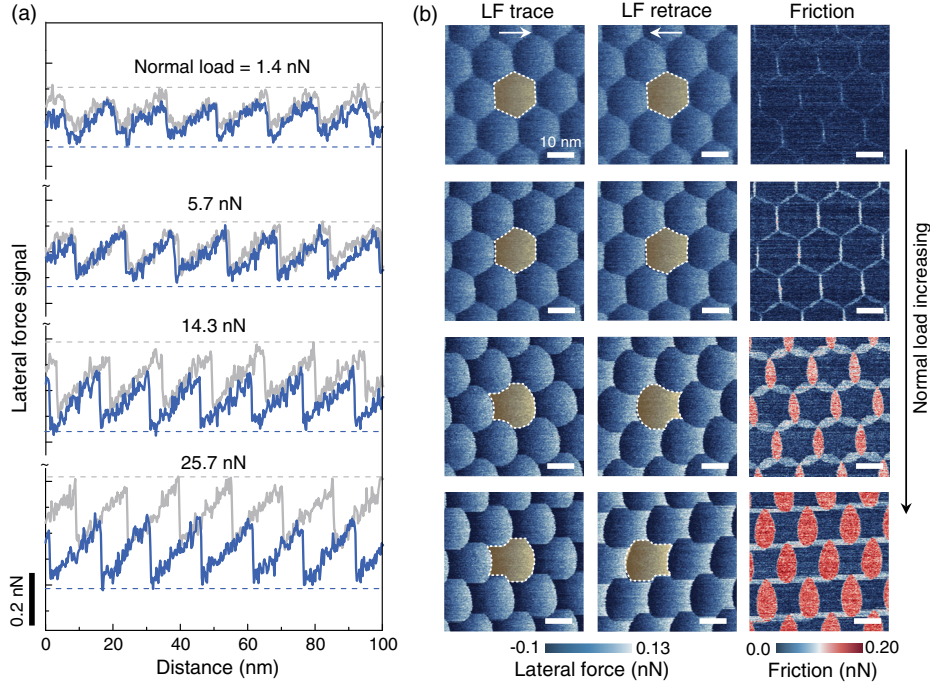


FIG. 2. (a) Trace (gray line) and retrace (blue line) lateral force curves obtained with a sliding velocity of $4 \mu\text{m/s}$ under normal loads of 1.4, 5.7, 14.3, and 25.7 nN, respectively. (b) The corresponding trace and retrace lateral force and friction images of (a). Scale bar, 10 nm.

cell of the moiré pattern becomes stretched along the fast scan direction as indicated by the dashed contour curves. Accompanied with this shape distortion, a significant phase shift between the trace and retrace signals, i.e., a higher degree of hysteresis, is also apparent under high loads. The sensitive dependence of the moiré-scale stick slip on normal load suggests that this long-range instability is associated with certain physical process critically influenced by loading of the tip. Recently, when measuring graphene/*h*-BN heterostructure using STM, Yankowitz *et al.* found that the upper graphene layer could be locally displaced and deformed along the in-plane direction due to pressure-induced commensurate stacking transition [32]. In our experiments, friction measurements were conducted under compressive normal loads and the AFM tip might perturb the graphene lattice similarly, which in turn would modulate the interaction potential between the AFM tip and graphene.

To properly understand the impact of the pressure-induced commensurate stacking transition on friction, the in-plane deformation of graphene has to be considered. Recently, to explain the layer-dependent friction and the strengthening behavior of graphene, Andersson *et al.* introduced an internal variable in the classic *P-T* model so that the extra degree of freedom of the graphene sheet could be considered [33]. Motivated by their work, we proposed an improved *P-T* model to incorporate the in-plane deformation of graphene. As schematically shown in Fig. 3(a), a particle, representing the AFM tip, is dragged via a spring with a force constant k_1 to move along a

potential energy landscape, representing the interaction between the tip and the heterostructure. The position of the particle and the spring based are denoted by x_1 and R , respectively. The deformability of the graphene layer is incorporated by considering the in-plane displacement of the graphene x_2 and an associated spring with a force constant k_2 . In this model, the interaction energy consists of two parts. The first part is the interaction energy between the tip and the upper graphene sheet U_{T-G} . Following the classic approach, $U_{T-G} = U_1 \cos(\theta_1)$, where U_1 is the amplitude of the energy corrugation and $\theta_1 = 2\pi(x_1 - x_2)/a_1$ is the relative energy phase at the tip position. The second part is the interaction energy between the graphene and *h*-BN interface, U_{G-B} . To consider the commensurability of the graphene and *h*-BN lattice, U_{G-B} is assumed to be $U_{G-B} = U_2 \cos(\theta_2)$, where U_2 is the energy prefactor and $\theta_2 = 2\pi(x_1/a_2 - x_1/a_1 + x_2/a_1)$ is the relative phase difference between the graphene lattice and the *h*-BN lattice at the tip position. Therefore, the total potential V of the tip-heterostructure system can be written as

$$V = U_{T-G} + U_{G-B} + U_{k_1} + U_{k_2}, \quad (1)$$

where $U_{k_1} = \frac{1}{2}k_1(x_1 - R)^2$ and $U_{k_2} = \frac{1}{2}k_2x_2^2$ are the elastic strain energy of the springs. With the modified system potential energy, we followed the classic approach and performed numeric simulations according to the Langevin-type equations (more details can be found in Supplemental Material [28]):

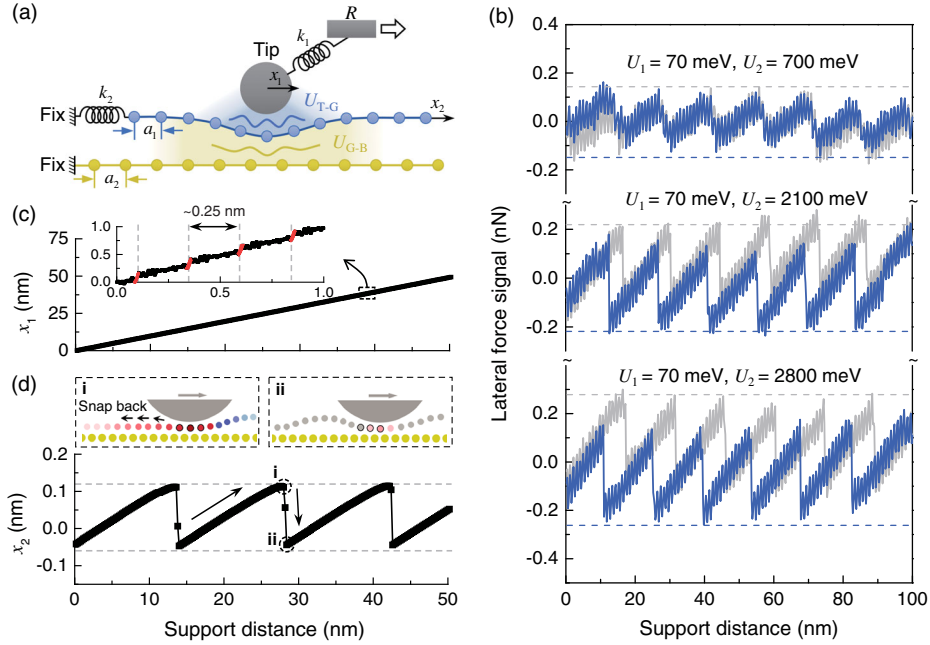


FIG. 3. (a) A schematic showing a tip sliding on a composite structure containing two periodic layers with different periods. The tip is moved by a support through a linear spring and the upper layer is fixed laterally through another linear spring. (b) Typical trace (gray line) and retrace (blue line) lateral force curves obtained in numerical calculations with $U_1 = 70$ meV, and varying U_2 of 700, 2100, and 2800 meV, respectively. (c) Variation of the tip displacement x_1 with the support displacement for $U_2 = 2800$ meV. Inset shows a magnified curve profile and the slip stages are highlighted with red segments. (d) Schematics showing the atomic configurations corresponding to two typical moments of (i) and (ii) as marked in the lower panel (upper panel). Variation of the upper layer displacement x_2 , with the support displacement obtained in numerical calculation with $U_1 = 70$ meV and $U_2 = 2800$ meV (lower panel).

$$\begin{aligned}
 m_1 \frac{d^2 x_1}{dt^2} - m_1 \gamma_1 \frac{dx_1}{dt} + \frac{\partial V(x_1, x_2, R)}{\partial x_1} &= \xi_1(t), \\
 m_2 \frac{d^2 x_2}{dt^2} - m_2 \gamma_2 \frac{dx_2}{dt} + \frac{\partial V(x_1, x_2, R)}{\partial x_2} &= \xi_2(t). \quad (2)
 \end{aligned}$$

Figure 3(b) shows a series of lateral force traces calculated from the improved P - T model when the graphene/ h -BN interaction energy is varied. In all cases, moiré-scale stick slip can be clearly seen in addition to the regular atomic-scale stick slip (see Supplemental Material, Fig. S5 [28]). Moreover, when U_2 is enhanced gradually, the peak force of the moiré-scale stick slip increases accordingly and the hysteresis between the trace and retrace curves also becomes more apparent. As increasing normal load will lead to stronger graphene/ h -BN interaction, the calculation qualitatively reproduces the evolutionary trend shown in Fig. 2.

To clearly illustrate the physical process behind this dual-scale stick slip, we extracted the variations of the tip displacement and graphene displacement from a typical numerical simulation. As shown in Fig. 3(c), when viewed at a large length scale, the tip seems to slide “continuously” as the base moves forward. However, the close-up view [the inset of Fig. 3(c)] indicates that the motion of the tip actually varies periodically corresponding to the

atomic-scale stick slip. In contrast to the “continuous” increase of the tip position, the graphene sheet instead oscillates periodically with a much longer period as shown in Fig. 3(d). During each cycle, the graphene sheet is gradually displaced in the in-plane direction and, until at some moment, the graphene sheet suddenly snaps back, as schematically illustrated in the upper panel of Fig. 3(d). The mechanism can be understood as follows. When the tip slides on the surface of graphene/ h -BN, the local stacking state tends to be commensurate under the tip pressure. Consequently, as the tip moves forward, the graphene will be gradually stretched in order to adapt to the lattice of h -BN and the interlayer interaction energy will increase (see more details in Supplemental Material, Fig. S6 [28]). When the deformation of graphene sheet becomes large enough, the graphene sheet will lose stability at a critical moment and suddenly snap back. The instability is governed by the competition between the in-plane strain energy of graphene and the graphene/ h -BN interfacial energy. As the latter term would change periodically with the position of the tip relative to the moiré structure, the resultant in-plane stretching and snap-back behavior was expected to occur with a period coinciding with the moiré pattern. Since the moiré-scale stick slip relies on local motion of graphene with respect to the h -BN, this unique behavior is affected by the interlayer interaction strength. According to

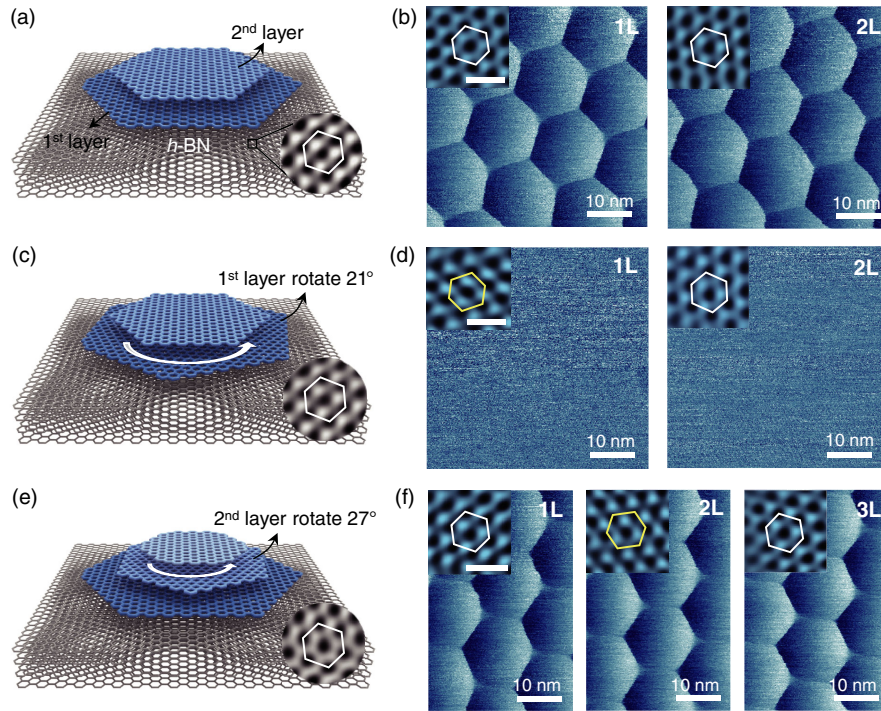


FIG. 4. (a) A schematic showing a bilayer graphene island on h -BN substrate. The bilayer graphene is aligned with h -BN. The inset shows the lattice orientation of h -BN. (b) Typical lateral force images obtained on the first and second graphene layers, showing clear moiré-scale stick-slip friction. Insets show the lattice orientation of the first and second graphene layers. Scale bar, 5 Å (inset). (c) A schematic showing a bilayer graphene island on h -BN substrate. There is a twist angle of 21° between the first graphene layer and h -BN, and the second graphene layer is aligned with h -BN. (d) Typical lateral force images obtained on the first and second graphene layers. Insets show the lattice orientation of the first and second graphene layers. Scale bar, 5 Å (inset). (e) A schematic showing a trilayer graphene island on h -BN substrate. There is a twist angle of 27° between the second graphene layer and h -BN. The first and third graphene layer are both aligned with h -BN. (f) Typical lateral force images obtained on the first, second, and third graphene layers. Insets show the lattice orientation of the first, second, and third graphene layers, respectively. Scale bar, 5 Å (inset).

Christian *et al.*, the interlayer interactions between graphene and substrates can be either physisorption with weak dispersion interaction or chemisorption with strong charge interaction [34]. If the graphene is strongly pinned by the substrate, then in-plane deformation of graphene is suppressed and the moiré-scale stick slip would be absent (see Supplemental Material, Fig. S7 [28]).

Since the moiré-scale stick slip originates from the dynamic behavior of the graphene/ h -BN interface, such a long-range friction modulation effect may persist for multilayer graphene. To test this idea, we grew multilayer graphene samples on h -BN substrates and we conducted friction measurements on different layers of these heterostructures. For the first sample shown in Fig. 4(a), a bilayer graphene island is grown h -BN. Based on the lattice-resolved AFM images, the crystalline orientations of the two graphene layers are aligned with the h -BN substrate. As shown in Fig. 4(b), moiré-scale stick-slip patterns can be clearly observed both on the 1L and 2L graphene. In contrast, for another bilayer graphene sample depicted in Fig. 4(c), where the first layer graphene is rotated by 21° with respect to h -BN but the second layer graphene is aligned with h -BN, no moiré-scale stick-slip pattern can be

observed either on 1L or 2L graphene as indicated in Fig. 4(d). This directly confirms that the moiré-scale stick slip is solely determined by the state of the graphene/ h -BN interface. Such a characteristic is further confirmed by the frictional behavior of a trilayer graphene/ h -BN sample. As schematically shown in Fig. 4(e), the first and third graphene layer of the trilayer sample are both aligned with h -BN but the second graphene layer has a 27° mismatch angle. Although both 1L/2L and 2L/3L interfaces are incommensurate, clear moiré-scale stick-slip patterns can be obtained on all graphene layers, as shown in Fig. 4(f).

In conclusion, friction on graphene/ h -BN superlattice structures was found to exhibit moiré-scale stick slip in addition to the traditional atomic-scale stick slip, resulting in unique length-scale dependent dissipation. Revealed by an improved PT model, we attributed the moiré-scale stick slip to the accumulation and sudden release of strain of the graphene layer. The finding gives the very example that the internal state of the van der Waals interfaces can have a profound impact on dynamics and energy dissipation mechanism of 2D heterostructures; and it also offers another tuning knob for regulating surface friction of a broad range of layer-structured materials.

We acknowledge the financial support from The National Natural Science Foundation of China (Grants No. 12025203, No. 11921002, No. 11890671, No. 51772317, No. 91964102, and No. 12004406), the Initiative Program of State Key Laboratory of Tribology (SKLT2022A01), the China National Postdoctoral Program for Innovative Talents (BX2021163, BX2021331), the Science and Technology Commission of Shanghai Municipality (Grant No. 18511110700), the China Postdoctoral Science Foundation (2021M701908), Soft Matter Nanofab (SMN180827) of ShanghaiTech University and the Shuimu Tsinghua Scholar program of Tsinghua University.

*To whom all correspondence should be addressed.
hmwang@mail.sim.ac.cn

†To whom all correspondence should be addressed.
qunyang@tsinghua.edu.cn

- [1] C. M. Mate, *Tribology on the Small Scale* (Oxford University Press, New York, 2008).
- [2] C. M. Mate, G. M. McClelland, R. Erlandsson, and S. Chiang, *Phys. Rev. Lett.* **59**, 1942 (1987).
- [3] W. F. Brace and J. D. Byerlee, *Science* **153**, 990 (1966).
- [4] O. Ben-David, S. M. Rubinstein, and J. Fineberg, *Nature (London)* **463**, 76 (2010).
- [5] Q. Li, T. E. Tullis, D. Goldsby, and R. W. Carpick, *Nature (London)* **480**, 233 (2011).
- [6] A. Socoliuc, E. Gnecco, S. Maier, O. Pfeiffer, A. Baratoff, R. Bennewitz, and E. Meyer, *Science* **313**, 207 (2006).
- [7] R. Capozza, S. M. Rubinstein, I. Barel, M. Urbakh, and J. Fineberg, *Phys. Rev. Lett.* **107**, 024301 (2011).
- [8] R. W. Carpick and M. Salmeron, *Chem. Rev.* **97**, 1163 (1997).
- [9] A. Vanossi, N. Manini, M. Urbakh, S. Zapperi, and E. Tosatti, *Rev. Mod. Phys.* **85**, 529 (2013).
- [10] A. Socoliuc, R. Bennewitz, E. Gnecco, and E. Meyer, *Phys. Rev. Lett.* **92**, 134301 (2004).
- [11] I. Szlufarska, M. Chandross, and R. W. Carpick, *J. Phys. D* **41**, 123001 (2008).
- [12] E. Gnecco, R. Bennewitz, T. Gyalog, and E. Meyer, *J. Phys. Condens. Matter* **13**, R619 (2001).
- [13] S. Y. Krylov, J. A. Dijksman, W. A. van Loo, and J. W. M. Frenken, *Phys. Rev. Lett.* **97**, 166103 (2006).
- [14] E. Gnecco, R. Bennewitz, T. Gyalog, C. Loppacher, M. Bammerlin, E. Meyer, and H. J. Güntherodt, *Phys. Rev. Lett.* **84**, 1172 (2000).
- [15] L. Jansen, H. Hölscher, H. Fuchs, and A. Schirmeisen, *Phys. Rev. Lett.* **104**, 256101 (2010).
- [16] Q. Li, Y. Dong, D. Perez, A. Martini, and R. W. Carpick, *Phys. Rev. Lett.* **106**, 126101 (2011).
- [17] I. Barel, M. Urbakh, L. Jansen, and A. Schirmeisen, *Phys. Rev. B* **84**, 115417 (2011).
- [18] Xin-Z. Liu, Z. Ye, Y. Dong, P. Egberts, R. W. Carpick, and A. Martini, *Phys. Rev. Lett.* **114**, 146102 (2015).
- [19] L. Prandtl, *ZAMM—J. Appl. Math. Mech./Z. Angew. Math. Mech.* **8**, 85 (1928).
- [20] G. A. Tomlinson, *London, Edinburgh, Dublin Philos. Mag. J. Sci.* **7**, 905 (1929).
- [21] Q. Li, Y. Dong, A. Martini, and R. W. Carpick, *Tribol. Lett.* **43**, 369 (2011).
- [22] R. Shi *et al.*, *2D Mater.* **4**, 025079 (2017).
- [23] X. Zheng *et al.*, *Nat. Commun.* **7**, 13204 (2016).
- [24] N. Chan, S. G. Balakrishna, A. Klemen, M. Moseler, P. Egberts, and R. Bennewitz, *Carbon* **113**, 132 (2017).
- [25] S. Maier, E. Gnecco, A. Baratoff, R. Bennewitz, and E. Meyer, *Phys. Rev. B* **78**, 045432 (2008).
- [26] T. Filleter, W. Paul, and R. Bennewitz, *Phys. Rev. B* **77**, 035430 (2008).
- [27] S. N. Medyanik, W. K. Liu, I.-H. Sung, and R. W. Carpick, *Phys. Rev. Lett.* **97**, 136106 (2006).
- [28] See Supplemental Material at <http://link.aps.org/supplemental/10.1103/PhysRevLett.128.226101> for details of sample preparation and measurements, improved Prandtl-Tomlinson model dynamics simulation, large-scale topographic and friction images, a TEM image of the tip, filtered atomic-scale lateral force images, lateral force curves and images obtained with varying sliding velocities, lateral force curves obtained under varying normal loads, lateral force curves obtained from numerical calculations, variation of the energy, and effect of the interfacial pinning capability, which includes Refs. [23, 24].
- [29] J. Liu, S. Zhang, Q. Li, X.-Q. Feng, Z. Di, C. Ye, and Y. Dong, *Carbon* **125**, 76 (2017).
- [30] Y. Song, D. Mandelli, O. Hod, M. Urbakh, M. Ma, and Q. Zheng, *Nat. Mater.* **17**, 894 (2018).
- [31] A. Vanossi, C. Bechinger, and M. Urbakh, *Nat. Commun.* **11**, 4657 (2020).
- [32] M. Yankowitz, K. Watanabe, T. Taniguchi, P. San-Jose, and B. J. LeRoy, *Nat. Commun.* **7**, 13168 (2016).
- [33] D. Andersson and A. S. de Wijn, *Nat. Commun.* **11**, 420 (2020).
- [34] M. S. Christian and E. R. Johnson, *J. Phys. Chem. C* **122**, 8910 (2018).